Applied Catalysis A, General 712 (2026) 120748

Contents lists available at ScienceDirect

Applied Catalysis A, General

journal homepage: www.elsevier.com/locate/apcata

Novel advanced channel reactor for spatio-temporal activity and catalyst state correlations applied for the reduction of NO by CO over Pt/Al_2O_3 ☆

Thomas Häber [a], Sui Wan [a], Samuel Struzek [b], Camilo Cárdenas [b], Anna Zimina [a], Florian Maurer [b], Patrick Lott [b], Rainer Suntz [b], Jan-Dierk Grunwaldt [a,b,*], Olaf Deutschmann [a,b,*]

[a] Institute of Catalysis Research and Technology (IKFT), Karlsruhe Institute of Technology (KIT), Hermann-von-Helmholtz-Platz 1, Eggenstein-Leopoldshafen, 76344, Germany

[b] Institute for Chemical Technology and Polymer Chemistry (ITCP), Karlsruhe Institute of Technology (KIT), Engesserstraße 20, Karlsruhe, 76131, Germany

ARTICLE INFO

Keywords:
Heterogeneous catalysis
Planar laser induced fluorescence (PLIF)
x-ray absorption spectroscopy (XAS)
NO reduction by CO
Correlating activity and state
Emission control

ABSTRACT

The correlation of space- and time-resolved measurements of catalytic activity with catalyst state is an invaluable tool to advance the understanding and development of complex catalytic systems under conditions relevant to technical applications. Such an approach is employed here to investigate the catalytic deactivation in the reduction of NO by CO over Pt/Al_2O_3 on freshly reduced catalysts in a channel reactor and at concentrations typical for emission control. Planar laser-induced fluorescence (PLIF) is used to visualize the 2D concentration profiles and to derive space- and time-resolved NO conversion rates for different CO/NO ratios, temperatures and mass flow rates. The changes in catalytic activity are correlated with temporal and spatial changes in oxidation state determined by *operando* X-ray absorption spectroscopy (XAS) under the same conditions. The time scales of the changes in catalytic activity depend not only on the stoichiometry and temperature, but also on the position along the catalyst channel and differ significantly from the temporal changes of the oxidation state. The different time scales are discussed in the context of the known CO poisoning as well as the formation and storage of isocyanate on the support. Isocyanate formation temporarily counteracting CO poisoning could explain the differences in the observed time scales under different reaction conditions and at different locations on the catalyst.

1. Introduction

Platinum group metals are often used in three-way catalysts to reduce emissions from mobile and stationary sources [1–6]. However, future stricter emission standards set by the government as well as other applications and sources for emissions [7] will increase the need for technical solutions to reduce emissions even further [1,2,8]. Over the past decades, extensive research has been conducted to investigate the performance of noble metal and transition metal catalysts in the reduction of NO by CO for gas purification [4]. Rhodium-based catalysts and bimetallic rhodium–platinum catalysts have been shown to be very effective for the reduction of nitrogen oxide [4,9,10], but due to the huge increase in cost and limited availability of rhodium [11], researchers have also looked extensively at other noble or transition metals [3,4,12,13].

A very well-known example is platinum on aluminum oxide (Pt/Al_2O_3), whose catalytic effect on the CO + NO reaction has been intensively studied for almost five decades [14]. Platinum (Pt) is a highly active [15] and compared to rhodium cheaper material [11] for the reduction of NO by CO. However, it has the highest light-off temperature among the platinum group metals [16] and forms significant amounts of N_2O depending on operating conditions and stoichiometry [15–18]. In addition, the catalytic activity decreases rapidly over time near stoichiometry and under net reducing conditions (excess CO) [15,17–19]. Mechanistically, the reaction involves non-dissociative adsorption of NO and CO, followed by the dissociation of NO (see Scheme 1) [14,15,20]. The dissociation of adsorbed NO at a free neighboring site is generally considered to be the rate-limiting step. However, the availability of reduced free Pt sites and not the intrinsic reaction rate of dissociation is probably the actual limiting factor [21],

☆ This article is part of a Special issue entitled: 'Luca Lietti 65th birthday' published in Applied Catalysis A, General.

* Corresponding authors at: Institute for Chemical Technology and Polymer Chemistry (ITCP), Karlsruhe Institute of Technology (KIT), Engesserstraße 20, Karlsruhe, 76131, Germany.

E-mail addresses: grunwaldt@kit.edu (J.-D. Grunwaldt), deutschmann@kit.edu (O. Deutschmann).

https://doi.org/10.1016/j.apcata.2025.120748
Received 30 June 2025; Received in revised form 18 November 2025; Accepted 13 December 2025
Available online 20 December 2025

$$\mathrm{Pt}\cdot + \mathrm{CO} \rightleftharpoons \mathrm{Pt\text{-}CO}$$

$$\mathrm{Pt}\cdot + \mathrm{NO} \rightleftharpoons \mathrm{Pt\text{-}NO}$$

$$\mathrm{Pt}\cdot + \mathrm{Pt\text{-}NO} \rightarrow \mathrm{Pt\text{-}N} + \mathrm{Pt\text{-}O}$$

$$\mathrm{Pt\text{-}CO} + \mathrm{Pt\text{-}O} \rightarrow \mathrm{CO_2} + 2\,\mathrm{Pt}\cdot$$

$$2\,\mathrm{Pt\text{-}N} \rightarrow \mathrm{N_2} + 2\,\mathrm{Pt}\cdot$$

$$\mathrm{Pt\text{-}NO} + \mathrm{Pt\text{-}N} \rightarrow \mathrm{N_2O} + 2\,\mathrm{Pt}\cdot$$

$$\mathrm{Pt\text{-}CO} + \mathrm{Pt\text{-}N} \rightleftharpoons \mathrm{Pt\text{-}NCO} + \mathrm{Pt}\cdot$$

$$\mathrm{Pt\text{-}NCO} \rightsquigarrow \mathrm{Al_2O_3\text{-}NCO} + \mathrm{Pt}\cdot$$

Scheme 1. Mechanistic steps for the reduction of NO by CO on Pt/Al_2O_3.

which supports the notion that inhibition by CO is the reason for the low catalytic activity in the presence of excess CO [15,17,21–24].

The well-known deactivation behavior and bi-stability of the CO + NO system over Pt/Al_2O_3 is accompanied by the formation of isocyanate (NCO) [18,21,22,25–29], which is formed on platinum (Pt-NCO) but quickly migrates to the support (Al_2O_3-NCO) (c.f. Scheme 1). Frank and Renken [17] found that catalyst pre-treatment with a CO/O_2 mixture, which potentially saturates the noble metal surface with adsorbed CO, did neither inhibit the high initial catalytic activity nor prevented its subsequent decrease over time. They suggested that the formation of isocyanate and its migration to the support removes CO from the metal surface, thereby counteracting the inhibiting effect of CO. However, the exact role of isocyanate in the reaction mechanism and its possible role in the catalytic deactivation is still discussed in the literature [15,17,18,22,30].

Although experimental results have been reported from a wide range of systems investigating the reaction of NO with CO over noble metal-based catalysts, experimental gas phase data from the literature has so far been limited to end-of-pipe concentrations. Non-invasive, optical measurement methods offer the possibility to follow the concentration profiles of selected species spatially and temporally resolved over layered catalysts. In this regard, planar laser-induced fluorescence (PLIF) is a highly sensitive, non-invasive standard diagnostic widely used in combustion research [31–34], that has gained considerable traction over the last two decades for studying the gas phase near catalytic surfaces [34–50]. Although PLIF is limited to certain types of molecules (e.g. OH, NO, NH_3, CO, NO_2, aldehydes), it allows the two-dimensional detection of the concentration field of a single species with a high time resolution, which is effectively limited only by the repetition rate of the laser and the desired signal-to-noise ratio. This enables the monitoring of catalytic activity as a function of space and time to elucidate the coupling between gas phase transport, surface kinetics and catalyst state. These aspects make PLIF a valuable extension to other existing spatially resolved methods, such as capillary based techniques [47,51–58] for studying spatial and transient concentration profiles, for example inside catalytic monoliths or in stagnation point reactors, coupled with mass spectrometry.

In recent decades, the catalyst structure, which is highly dependent on operating conditions and mass transfer properties, and its modeling have been investigated separately in most cases. The advantage of monitoring the spatial activity, as offered by PLIF, in conjunction with spatially and temporally resolved information about the state of the catalyst in a chemical reactor is that structure–activity correlations can be determined. This also enables the creation of numerical models, as these models can be verified. X-ray absorption spectroscopy (XAS) is a common measurement method for identifying the structure of small precious metal particles and clusters. In particular, it enables the determination of the chemical state, both spatially and temporally resolved [59–62]. XAS is also a non-invasive technique that can be used for *operando* experiments in various reactors with a spatial resolution in the mm range and a temporal resolution of several seconds to several minutes. In recent years, spatially resolved XAS investigations have attracted a lot of attention because it has become possible to measure the X-ray absorption structure near the edge (XANES) in 2D [62,63] and recently even in 3D [64].

In this work we report on measurements of local gas phase concentrations directly above a plate coated with Pt/Al_2O_3 in the reaction of NO with CO using planar laser-induced fluorescence (PLIF) to elucidate the space and time-resolved catalytic activity over a broad range of conditions. The detection of the entire NO concentration field above the catalyst layer offers the unique possibility to extract local NO conversion rates. Depending on the stoichiometry and to a lesser extent on the temperature, the temporal evolution of the NO conversion rate and of catalytic activity is shown to differ significantly when moving from the inlet to the outlet along the catalyst plate. Using a newly developed channel reactor, the gas phase measurements are complemented by time-resolved X-ray absorption spectroscopy (XAS) measurements that were conducted at different points along the plate to follow the temporal evolution of the Pt oxidation state of the catalyst during the decline of catalytic activity. Finally, the different temporal evolution of catalytic activity and electronic state of Pt at comparable positions, as well as the potential role of isocyanate, is discussed.

2. Experimental

2.1. Sample preparation

In our investigations, the catalyst was prepared using an automated incipient wetness impregnation technique (CATIMPREG, Chemspeed Technologies AG) described previously [65,66] using tetraamineplatinum(II) nitrate (Fischer Scientific, 99.99 %) and a commercial aluminum oxide support (Sasol Puralox TH 100/150). The resulting Pt/Al_2O_3 powder catalyst sample was calcined for 5 h at 500 °C in static air. The final platinum loading amounted to 1.88 ± 0.10 wt.-% as determined by ICP-OES (Inductively Coupled Plasma-Optical Emission Spectrometry) and the BET surface area was $136\,m^2/g$. TEM

investigations revealed an average noble metal particle size of 2.0 nm (±0.9 nm), which corresponds to a dispersion of about 56%, assuming ideal hemispherical particles [67]. Based on this catalytic material, an aqueous suspension (slurry) with 10 wt.-% Disperal P2 (Sasol) as binder was made and applied to the respective stainless steel plates (see below) as a carrier. The catalytically coated plates were calcined again for 5 h at 550 °C in air.

Before each measurement, the catalytic plate is pre-treated/conditioned inside the reactor to clean and activate the Pt surface by: (1) Oxidation with 10 vol.-% O_2 in N_2 (or He) at 450 °C for one hour. (2) Reduction with 5 vol.-% H_2 in N_2 (or He) at 400 °C for two hours. After conditioning, the catalyst is kept under an inert gas flow (1 L/min N_2 or He) until the start of the actual measurement. At that point, the inlet gas flow is switched from inert gas to the reactive gas mixture (200 – 800 ppm CO and 400 ppm NO in N_2 or He) using either two 3/2-way solenoid valves (Bürkert) or a single pneumatically actuated 4-way valve (Swagelok, Series 43) in the PLIF or XAS setup, respectively. Gases are supplied to the reactors by mass flow controllers (Bronkhorst). Except when noted otherwise, all experiments are conducted at atmospheric pressure, with a total flow rate of 1 L/min (NTP ≡ 1 atm & 20 °C).

2.2. PLIF setup

The experimental setup for the channel experiments is identical to that described previously [37,44]. An 18 mm wide and 25 mm long plate cut from a cordierite honeycomb structure is coated with the catalyst powder using the coating method described previously [50] and placed flush with the inner channel wall into a recess and in the center of a ceramic block forming a 2 mm high and 18 mm wide channel with a total length of 150 mm. The ceramic channel is placed inside a quartz tube, sealed with two steel caps, and heated by heating coils (HORST) using a PID controller (Eurotherm).

Detection of NO by planar laser-induced fluorescence (PLIF) is realized by exciting the $P_2(12.5) + Q_{12}(12.5)$ line in the $A^2\Sigma – X^2\Pi(0,0)$ rovibronic band at 226.7 nm [68], and collecting the fluorescence through an image-intensified charge-coupled device (ICCD) camera (IRO 25 & Imager QE, LaVision) equipped with a band pass-filter at 248 nm (FWHM = 10 nm, peak transmission 15 %, LaVision) [37]. The excitation laser is generated from the fundamental of a tunable dye laser at ≈627.0 nm (PrecisionScan, Sirah) pumped by the second harmonic of a 10 Hz Nd:YAG laser (Quanta-Ray Pro, Spectra-Physics), with subsequent sum frequency mixing of the dye laser output with the third harmonic of the same Nd:YAG laser. Using a set of lenses, the laser beam is transformed into a thin light sheet (~150 µm thick), oriented parallel to the flow direction and vertical to the catalytic plate. This allows capturing the 2D NO concentration field above the plate and over the full height of the channel. The fluorescence intensity S_F is generally governed by [69]:

$$S_F = C I_0 x_{NO} \frac{N_A p}{k_B T} B_{12} f_B(T) \frac{A_{21}}{A_{21} + Q_{21}(x_p, T)} \quad (1)$$

where C is an experimental constant which describes the optical system, I_0 is the local laser intensity, x_{NO} the mole fraction of NO, B_{12} and A_{21} are the Einstein coefficients for absorption and spontaneous emission, respectively, $f_B(T)$ is the Boltzmann population fraction of the excited energy level, $Q_{21}(x_p, T)$ the collisional quenching rate and x_p the mole fractions of the quenching species. N_A, p, k_B and T are the Avogadro constant, pressure, Boltzmann constant and temperature, respectively, which relate the particle number density ^1N to the mole fraction: $^1N = x_{NO} N_A p/(k_B T)$. At the low concentrations investigated here, changes in I_0 due to absorption along the catalyst plate can be neglected, so that only x_{NO} and Q_{12} depend on the local reactant concentrations.

Quantitative NO PLIF is achieved by adding 2 vol.-% CO_2 as the dominant fluorescence quencher to the gas mixture to keep the collisional quenching rate essentially independent of the reactant concentrations throughout the whole channel. The quenching cross section of CO_2 is similar to that of NO and much larger than any of the other components in the gas mixture [69]. Powder bed reactor tests (not shown here) with and without CO_2 addition confirmed that adding excess CO_2 does not have a significant impact on the results. Dividing the fluorescence signal S_F by a fluorescence image of a known NO concentration (non-reactive case) at the same temperature takes into account experimental factors such as the spatial intensity profile of the laser, optical filters, solid angle of fluorescence signal detection and spectral detection sensitivities as well as the temperature dependencies. All measurements are conducted with the laser intensity and NO concentration in the linear regime ($F \sim I_0$ and $F \sim x_{NO}$). In addition to the in-situ detection of NO using PLIF, a Fourier-transform infrared spectrometer (FTIR) (Series 2000, MKS) is connected to the reactor to monitor the NO, N_2O, NO_2, CO and CO_2 concentrations at the outlet.

2.3. Advanced channel reactor

A new reactor was developed to enable *operando* X-ray absorption spectroscopy in fluorescence mode on flat layered catalysts in a thin channel, with a flow pattern and catalyst geometry very similar to that of the PLIF setup described in the previous section, but with the potential of performing PLIF and XAS measurements simultaneously in the next design iteration. It is designed to provide an undisturbed laminar flow with minimal dead volume, which is suitable for rapid gas changes at the inlet or pulsing experiments. A sufficiently large, thermally insulated stainless steel body provides enough thermal inertia to allow stable operation even in highly exothermic reactions over a wide temperature range, while also enabling light-off measurements at heating rates of 2 K/min and temperatures up to 550 °C. An extensive elucidation of the thermal stability and temperature distribution within the reactor is provided in the supplementary material.

Fig. 1 shows a 3D rendering of a sectional view of the reactor to illustrate the channel geometry as well as a cross-sectional slice in the xz-plane. The reactor consists of a heated stainless steel frame and the actual channel is formed by replaceable inlays to allow for an easy replacement of the catalyst plate as well as to accommodate plates of different sizes. All internal parts in contact with the gas phase have been plasma-coated with Al_2O_3 to suppress side reactions on metal surfaces. The reactor is heated by four mineral-insulated, 2-core heating wires with seamless cold ends (150 W per wire, ThermSys GmbH), embedded on all four sides of the stainless steel casing. Thermocouples (TC) are placed as close as possible to the catalytic layer and at different positions throughout the reactor body to monitor the temperature distribution inside the reactor. All four heating wires are controlled by a single, programmable PID controller (Eurotherm, model 3208).

Access to X-rays is provided by a 5 mm wide and 80 mm long slit and two layers of thin aluminum foil (thickness about 10 µm) above the catalyst plate. The inner foil constraints the geometry of the channel (height 2 mm) and the outer foil seals the reactor against the environment.

2.4. XAS setup

XAS measurements were conducted at the CAT-ACT beamline of the KIT Light Source (Eggenstein-Leopoldshafen, Germany) [70] in the newly developed advanced channel reactor described in the previous subsection. A dual channel monochromator with a pair of Si(111) crystals was used to select the photon energy for the experiments. The incoming X-ray beam penetrated the X-ray windows made by Aluminum foil at an angle of roughly 45° as shown in Fig. 1. The in total 28 µm of Al foil in the X-ray beam decreases the overall photon flux by approximately 12% at the Pt L_3 edge (11564 eV). The

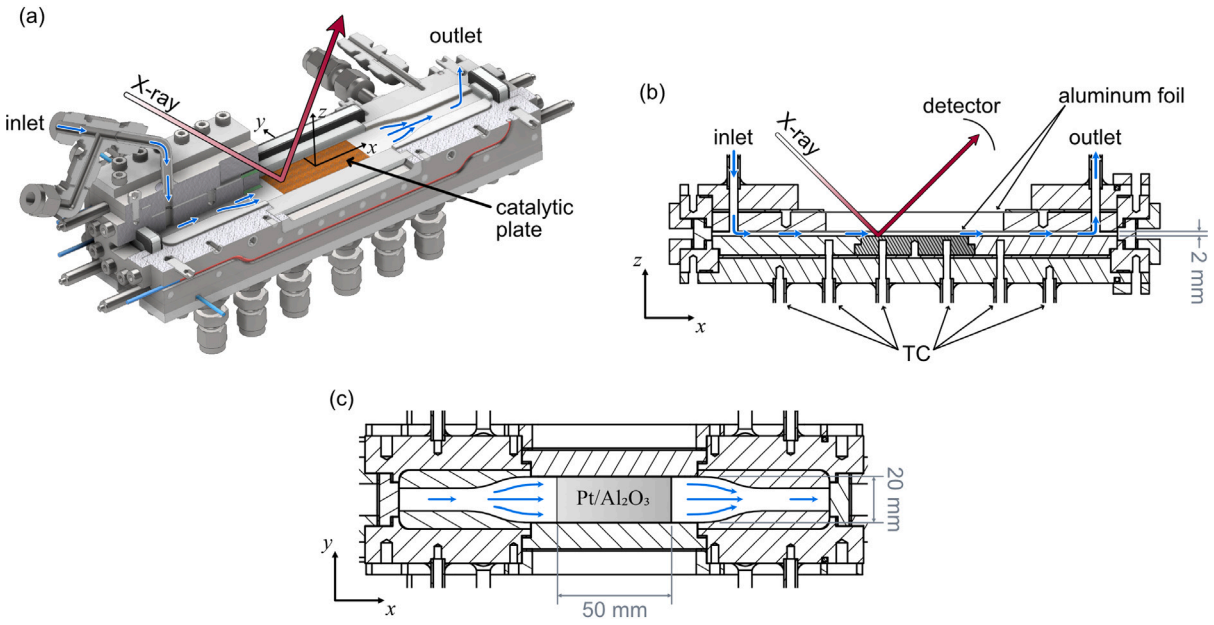

Fig. 1. (a) Sectional 3D-view of the new channel reactor for XAS measurements. The catalyst-coated plate (20 mm × 50 mm) is positioned at the center of the channel in the direction of flow. (b) Cross-section in the xz-plane. The X-ray beam enters the reactor through a 5 mm wide and 80 mm long slit in the reactor body and allows the detection of X-ray fluorescence at an angle of up to 90° relative to the X-ray beam. (c) Top view with gas flow indicated in blue.

emitted fluorescence radiation exhibited an angle of approximately 45° as well. Vertical and horizontal slits were used to set a beam size of 1 mm × 2 mm, respectively. Fluorescence radiation was detected by a Si solid state detector (1E-Vortex, Hitachi High-Tech America, Inc.). XAS spectra of the Pt L_3 edge were recorded in the energy range from 11.48 keV to 11.91 keV, with each complete scan taking about 2 min. The XANES spectra were normalized by setting the regions of constant signal intensity at low and high energies to 0 and 1, respectively (see Fig. S3 in the supplementary material for details). The data analysis was conducted by linear combination fitting (LCF) with Python. For this, the spectrum after catalyst treatment in H_2 was used as reference for the reduced state, hereafter referred to as Pt reference, and the spectrum after treatment in O_2 was used as oxidized reference, hereafter referred to as PtO_2 reference. This approach ensures that small deviations due to the small particle/cluster size between the spectra of bulk Pt or PtO_2 and reduced or oxidized Pt nano-particles, respectively, do not bias the data evaluation. Gases were dosed by mass flow controllers (EL-Flow Select, Bronkhorst) and analyzed after the reactor outlet by a mass spectrometer (OmniStar, Pfeiffer) and Fourier-transform infrared spectroscopy in a flow through gas cell (Gasmet DX400, Gasmet Technologies GmbH).

The catalyst plate itself is a stainless steel slab (20 mm wide and 50 mm long) with an Al_2O_3 plasma coating on the top, which is further covered with the actual catalyst layer. The latter is deposited in layers using an airbrush pistol, with each layer being allowed to dry at a slightly elevated temperature (approx. 35 °C) before the next layer is applied. A total of approx. 10–15 layers are applied, which corresponds to a total specific Pt/Al_2O_3 surface loading of approx. 54 µg/mm^2. The homogeneity of the layer coating was confirmed *via* a XANES line scan along the catalyst. (See ESI for more information).

3. Results

3.1. Local conversion rates (PLIF)

Experiments measuring the spatio-temporal evolution of the catalytic activity between 250 °C and 450 °C and with varying stoichiometry were performed using PLIF, which provides quantitative measurements of the NO gas phase concentration directly above the catalytic plate inside the 2 mm high channel reactor as a function of space and time. Prior to each measurement, the sample is conditioned and then kept in an inert environment by flowing N_2 (1 L/min). At $t = 0$ min, the feed stream is switched to the corresponding CO/NO mixture, which also contains 2 vol.-% CO_2 to neglect local variations in quenching rates (see experimental section) and is balanced by N_2. As an illustrative example, Fig. 2 shows the local NO concentration distribution over the entire height of the channel at different times after the onset of the reaction. PLIF images were recorded continuously for 30 min at a repetition rate of 10 Hz. To improve the signal-to-noise ratio (SNR), the images are averaged over 100 continuous laser shots for each time point shown. Since the decline in catalytic activity occurs over a time frame of a few tens of minutes, the change in concentration within 10 s is negligible. The position of the catalyst is marked by a hatched area and ranges from $x = 0$ mm to 25 mm. The observed NO concentration gradients in flow and wall normal direction are due to the interaction between catalytic surface reactions (consumption of NO at the catalytic layer at $z = 0$ mm) and the diffusive and convective mass transport in the channel flow. A decrease in catalytic activity over time is directly reflected in a reduced overall NO concentration gradient in flow direction, as can be seen from the downstream shift of the NO concentration iso-lines as time progresses (indicated by arrows in Fig. 2).

The known decline in the catalytic activity [15,17–19] over fresh Pt/Al_2O_3 is also evident from the integral catalytic conversion $|\Delta x_j|$ at the reactor outlet, which is shown in Fig. 3 for stoichiometric and net reducing conditions and which was determined in parallel to the PLIF measurements using FTIR. The conditions are identical to those in Fig. 2. Here, $|\Delta x_j|$ is the consumption of reactants (CO and NO) or the formation of the IR-active product N_2O, where x_j is the mole fraction of species j and $\Delta x_j = x_{j,out} - x_{j,in}$ is the concentration difference between reactor outlet and inlet. NO_2 was not observed under the conditions investigated here. Overall, the decline in catalytic activity depends strongly on the CO/NO ratio and is considerably faster with an excess of CO. In addition, the temporal development of the N_2O concentration, a harmful greenhouse gas, is also different. While N_2O rises slowly under stoichiometric conditions, it quickly reaches a maximum under excess CO conditions, followed by a slow decline. An important factor influencing N_2O formation is the surface coverage

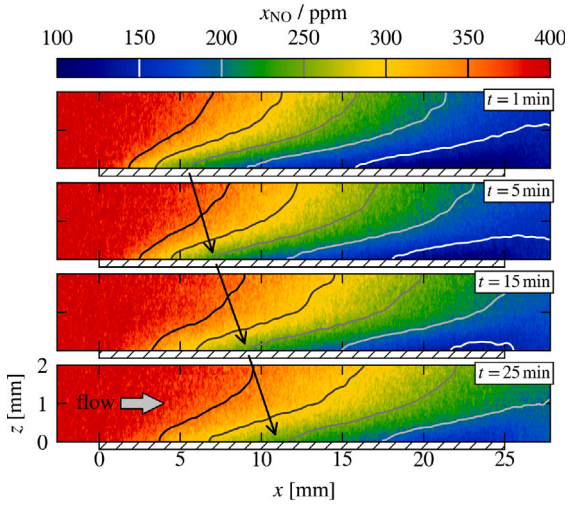

Fig. 2. Temporal development of the two-dimensional NO distribution over a catalyst-coated plate under stoichiometric conditions. The geometric location of the catalytic plate is marked with a hatched area and extends from $x = 0$ mm to 25 mm. (350 °C, 1 L/min, 400 ppm NO, 400 ppm CO, 2% CO_2, rest N_2).

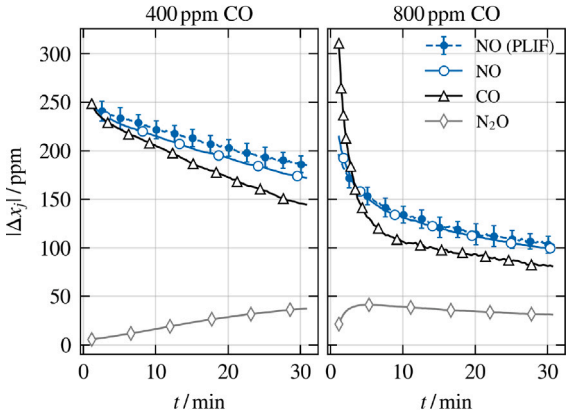

Fig. 3. Time evolution of the integral consumption of reactants (CO and NO) and formation of N_2O at the outlet of the channel reactor measured using FTIR at stoichiometric and net reducing conditions. Also shown is the NO consumption directly obtained from the PLIF images. (350 °C, 1 L/min, 400 or 800 ppm CO, 400 ppm NO, 2% CO_2, rest N_2).

ratio [NO*]/[N*], which requires the presence of only partially reduced Pt sites to catalyze the dissociation of NO into adsorbed N and O while preventing complete NO dissociation [13,17,20,71,72].

Fig. 3 also shows the integral consumption of NO directly obtained from the PLIF measurements by averaging the NO concentration distribution upstream (inlet, $x < 0$ mm) and downstream (outlet, $x > 25$ mm) of the catalytic plate. Error bars represent the 3σ-standard deviation of the PLIF signal in those regions, so they only reflect the statistical uncertainty of the detection system. On an absolute scale the NO integral consumption obtained from FTIR and PLIF agree quite well, verifying our approach to obtain quantitative NO concentration fields using PLIF with sufficient precision.

In terms of species balances, the conversion of NO at the catalytic plate is a sink for NO, resulting in a concentration gradient in the direction perpendicular to the plate. Since the mass flow and temperature are constant, the convective mass transport and the diffusion coefficient remain also constant. Therefore, the local concentration gradient at the plate reflects the local NO consumption rate R_{NO}:

$$R_{NO} \sim D_{NO} \frac{p}{RT} \left(\frac{dx_{NO}}{dz} \right)_{z=0} \tag{2}$$

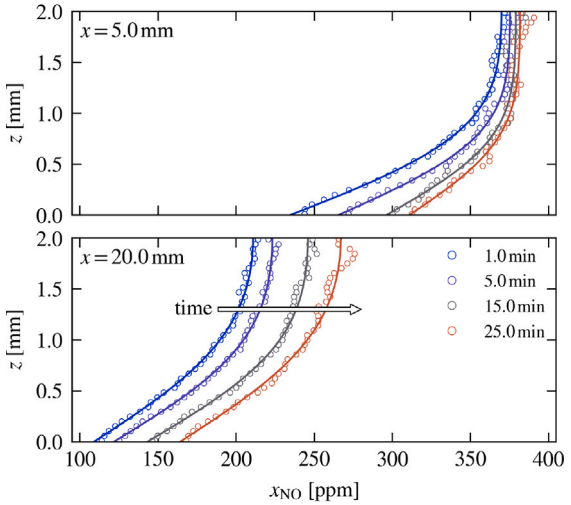

Fig. 4. Wall normal slices at $x = 5$ mm and 20 mm and at different times after the onset of the experiment. Solid lines are fitting curves according to Eq. (3). (350 °C, 1 L/min, 400 ppm NO, 400 ppm CO, 2% CO_2, rest N_2).

where D_{NO} is the mixture-averaged diffusion coefficient of NO. Conversely, the wall-normal concentration gradient at the upper (non-reactive) wall should be zero: $(dx_{NO}/dz)_{z=2\,mm} = 0$. Fig. 4 shows concentration profiles perpendicular to the plate at two positions along the plate, $x = 5$ mm and 20 mm, and for the same time points as in Fig. 2. For the visualization, the vertical profiles were averaged in time intervals of 10 s and in spatial intervals of 1 mm along the x-direction. Taking the noise into account, the concentration gradient at the upper, non-reactive wall is indeed approximately zero, while the concentration decreases in the direction of the catalytic surface at $z = 0$ mm.

Since all measurements were performed under isothermal conditions and both the change in number density due to reactions and axial diffusion are negligible in respect to the overall flow, the velocity profile along the channel remains the same. In this case, the wall-normal concentration profiles can be fitted to a functional form, which is commonly found in 1D diffusion problems with Dirichlet and/or Neumann boundary conditions [73]:

$$x_{NO}(z) = x_{s,NO} + 4\beta \sum_{n=1}^{\infty} \frac{\sin\left((2n-1)\pi \frac{z}{2h}\right)}{(2n-1)\pi} \exp^{-(2n-1)^2\pi^2\tau} \tag{3}$$

where $x_{s,NO}$, β and τ are fit parameters, h is the height of the channel and z the distance from the catalytic surface. Apart from $x_{s,NO}$, which represents the NO concentration near the surface, the fitting parameter β and the dimensionless time scale τ have no directly applicable physical interpretation in this context. The purpose of Eq. (3) is merely to provide a functional form that reflects the physical process to analyze the gas phase concentrations as well as the concentration gradients near the catalytic surface.

Solid lines in Fig. 4 represent fits to Eq. (3), which also aid to better visualize the evolution of the concentration gradients close to the catalytic surface. At $x = 5$ mm, a significant decrease in the near-wall NO concentration gradient can be observed, indicating that the NO consumption rate at the upstream position decreases significantly over time. In contrast, the gradient at the downstream position ($x = 20$ mm) appears to be invariant over the measured period (almost parallel lines). However, the absolute NO concentration near the wall still increases with time. Considering that the local conversion rate is approximately proportional to the local gas phase concentration ($R_{NO} \sim x_{NO}$) [14,15,18], this means that the catalytic activity also decreases at the downstream position, albeit at a slower rate.

Fitting Eq. (3) to the wall-normal concentration profiles at each time step t and at each position x along the plate and then inserting into

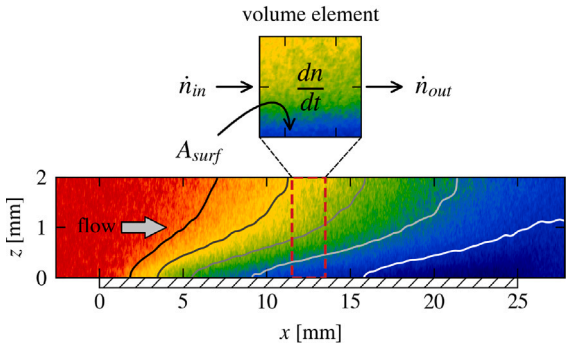

Fig. 5. Sketch of the volume elements used to estimate the NO consumption rate by means of a volumetric species balance.

Eq. (2) provides a measure of the space- and time-resolved consumption rate of NO. Because the PLIF images cover the entire height of the catalytic channel, the NO consumption rate can also be derived using a volumetric species balance independently. For this purpose, the gas phase is divided into small volume elements in the direction of the flow. The height of each volume element corresponds to the full height of the channel (see Fig. 5). Since no gas phase reactions take place at the temperatures considered here, the catalytic consumption rate of NO is simply the difference between the molar fluxes entering and leaving the volume elements:

$$R_{\mathrm{NO}} = -\frac{\dot{n}_{out} - \dot{n}_{in}}{A_{surf}} \tag{4}$$

Here A_{surf} is the geometric surface area of the catalytic plate underneath the volume element and $\dot{n}_{in}$ and $\dot{n}_{out}$ are the total molar fluxes of NO entering and leaving the volume element.

A comparison of the space- and time-resolved consumption rates $R_{\mathrm{NO}}(x,t)$ obtained with both methods, namely Eq. (2) and (4), is shown in Fig. 6, again at 350 °C and for stoichiometric and net reducing conditions. Consumption rates are plotted at the same points in time as in Fig. 4. Temperature dependent diffusion coefficients D_{NO} were calculated using the kinetic theory for transport properties as implemented in the Cantera software package [74] and which match diffusion coefficients of NO in N_2 reported in the literature [75]. The first thing to note is that the consumption rate derived from the wall normal concentration gradient is smaller by a factor of about 2.2 compared to the values derived from the volumetric balance. To facilitate a better visual comparison, the first has been scaled to match the latter in Fig. 6.

From an analytical point of view, both methods have their strengths and weaknesses. A more detailed discussion of the factors that influence the resulting conversion rates and which are responsible for the factor 2.2 can be found in the supplementary material (c.f. Fig. S5). The most important result, however, is that the variation of the NO consumption rate as a function of time and location along the catalytic plate is practically identical for both methods. Therefore, if only the changes in relation to a specific position or time are considered, the method based on diffusion fluxes is equivalent or even advantageous, given its better temporal and spatial resolution. On the other hand, the rates can also be easily scaled to the integral consumption rates measured simultaneously via FTIR in order to obtain absolute spatially and temporally resolved conversion rates with an accuracy better than ±20 %.

From Fig. 6 it is immediately obvious that the NO conversion rate varies along the catalytic plate. Additionally, the temporal and spatial behavior of the NO conversion depends strongly on the reaction conditions. When interpreting spatio-temporal changes in the net conversion rates of NO, the influence of the local gas phase concentration, which also changes with time and along the catalyst, must always be taken into account. Granger et al. measured the global conversion rates at

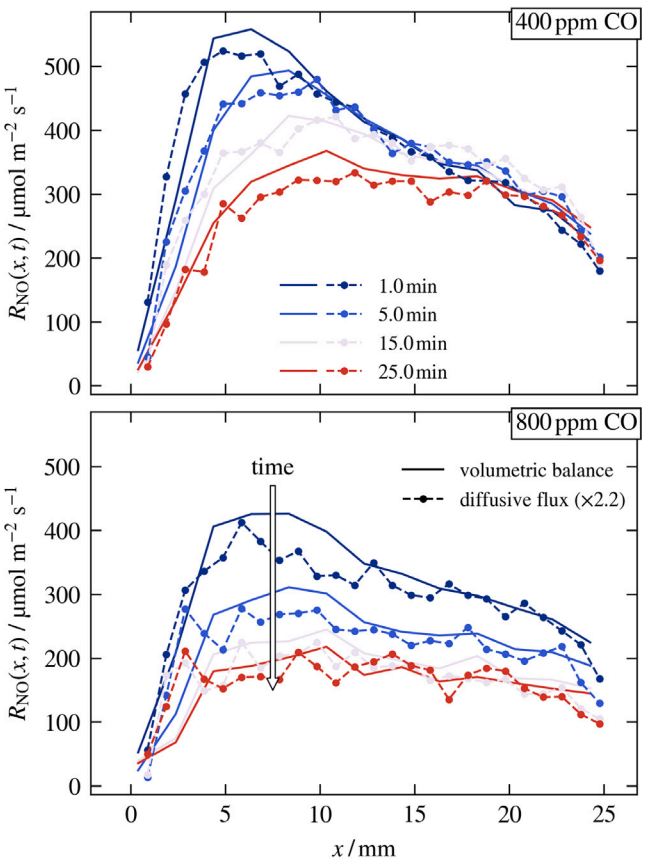

Fig. 6. Space and time-resolved consumption rates of NO derived from wall normal concentration gradients (1 mm and 10 s intervals) and a volumetric balance (2 mm and 60 s intervals) for stoichiometric (400 ppm CO) and net reducing conditions (800 ppm CO). (350 °C, 1 L/min, 400 ppm NO, 2% CO_2, rest N_2).

similar CO/NO ratios and temperatures over Pt/Al_2O_3 and found that the reaction order with respect to NO is close to one [15]. Similar results were obtained by Lorimer and Bell for Pt/SiO_2 [18]. This is also consistent with global kinetic models based on the generally accepted assumption that dissociation of adsorbed NO is the rate-limiting step [14,15]. Although, strictly speaking, these models are only valid under steady-state conditions, the decrease in activity over time is much slower than the chemical time scales of the relevant reactions involved. Therefore, for all reactions except those responsible for the slow accumulation of surface species, and similar to our previous experimental and numerical studies of nitrogen storage catalysts [44,49], steady-state assumptions continue to apply for each time step. Most of the effects due to changes in local gas phase concentrations can therefore be accounted for by taking the ratio between the net NO conversion rate R_{NO} and the NO concentration $c_{s,\mathrm{NO}}$ near the surface. The latter is easily available by fitting the wall-normal concentration profiles plotted in Fig. 4 to Eq. (3): $c_{s,\mathrm{NO}} = x_{s,\mathrm{NO}} \times p/(RT)$.

The ratio $R_{\mathrm{NO}}/c_{s,\mathrm{NO}}$, which is a more direct measure of the *intrinsic* activity, is shown in Fig. 7 for the same conditions as before. When there is an excess of CO (800 ppm CO, 400 ppm NO), the activity decreases over the entire length of the catalyst in the first few minutes, indicating that the catalytic state is the same at any position on the plate at any given time. In contrast, under stoichiometric conditions (400 ppm CO, 400 ppm NO), spatial gradients of the activity become apparent in addition to the temporal dependence. Near the inlet, the activity decreases very quickly, similar to that observed with an excess of CO, but a rather slow yet clearly visible decrease in activity can also

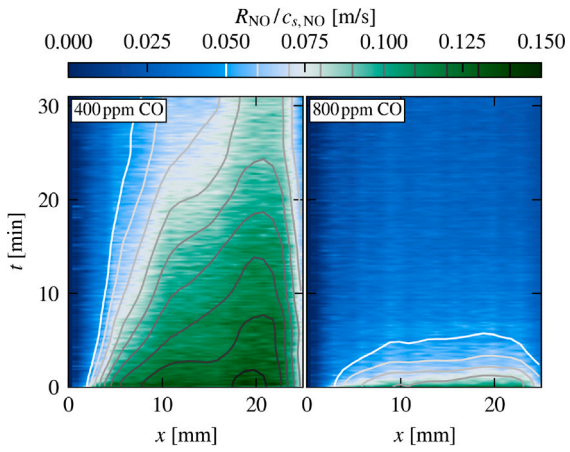

Fig. 7. Spatio-temporal variation of the catalytic activity under stoichiometric (left) and net reducing conditions (right). (350 °C, 1 L/min, 400 or 800 ppm CO, 400 ppm NO, 2% CO_2, rest N_2).

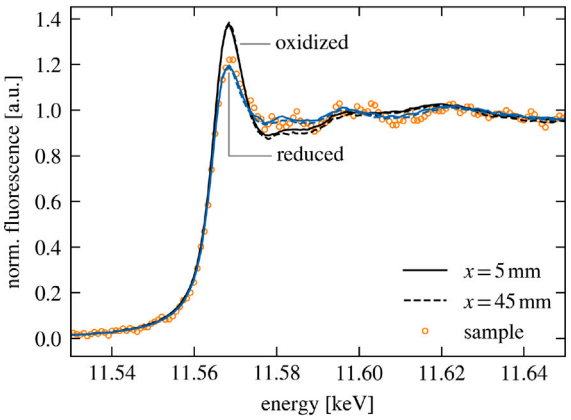

Fig. 8. Pt L_3 edge XANES reference spectra of Pt and PtO_2 particles recorded during oxidative and reductive conditioning of the catalyst (averaged over at least 30 scans). The reference spectra obtained near the inlet (x = 5 mm) and outlet (x = 45 mm) are practically identical. A typical example spectrum (in excess of CO) is shown with orange dots to illustrate the signal-to-noise ratio and its state.

be observed close to the outlet. Similar temporal and spatial changes as well as the same strong differences between stoichiometric conditions and those with an excess of CO were observed for all investigated temperatures (see Figure S6 in the supplementary information).

3.2. Catalyst state (XAS)

To gain insight into the state of the catalyst during these spatial and temporal changes, we performed time-resolved X-ray absorption spectroscopy under very similar conditions using the new XAS channel reactor that is also suited for PLIF. For both the PLIF and XAS measurements, the same catalyst powder was used to prepare the catalytic plates and an identical pre-treatment (oxidation with 10% O_2 at 450 °C and reduction with 5% H_2 at 400 °C) was applied to remove all pre-adsorbed species on the catalytic surface and to start each measurement from a unique catalytic state. Furthermore, the geometry of the catalytic channel in the XAS measurements is essentially the same as in the PLIF measurements, with the only difference that the Pt/Al_2O_3-coated plate is now twice as long, namely 50 mm instead of 25 mm. The catalyst plate is oriented so that the X-ray beam lies in the xz-plane (c.f. Fig. 1) and is positioned to examine points 5 mm from the beginning or end of the plate, i.e. at $x = 5$ mm and 45 mm respectively. XAS spectra recorded during oxidative and reductive pre-treatment and averaged over at least 30 scans (approx. 1 h of acquisition time) serve as reference spectra in the following analysis (see Fig. 8) Note that the reference spectra obtained at different positions of the catalyst are practically identical, which underscores that the coating is uniform (c.f. Fig. S4 in the supplementary information) and no gradients occur after oxidative or reductive pre-treatment. A single sample spectrum obtained with an excess of CO is also shown in Fig. 8 to illustrate the signal-to-noise ratio in the XANES scans at the selected time resolution of 2 min. The root-mean-square (RMS) value of the noise level of the normalized spectra is approximately 0.02.

Fig. 9 shows the results of the XAS studies for the same two conditions that proved to be of particular interest in the PLIF studies. As before, after pre-treatment, the catalyst is kept under a constant N_2 flow of 1 L/min until at $t = 0$ min the feed flow is switched to a near stoichiometric (left column) or net reducing (right column) CO/NO mixture balanced by N_2. To verify that the XAS channel reactor provides similar results to those in the previous section, the top row of Fig. 9 first shows the N_2O formation as an example, for which the temporal evolution is very sensitive to the reaction conditions and which was measured with an FTIR at the outlet of the reactor, simultaneously to the XAS spectra. In comparison to Fig. 3, it is clear

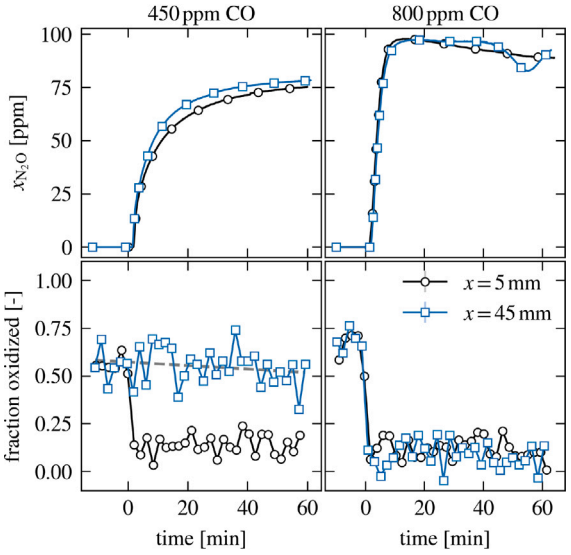

Fig. 9. Time-resolved evolution of the oxidation state measured at two different positions along the catalytic plate (bottom row) as well as the integral formation of N_2O (top row) for near stoichiometric (left) and net reducing conditions (right). (350 °C, 1 L/min, 450 or 800 ppm CO, 400 ppm NO, rest N_2).

that the temporal behavior of the N_2O evolution closely matches that of the PLIF channel reactor. For example, under stoichiometric conditions, the N_2O evolution slowly increases over the entire measurement time, while under net reducing conditions it quickly increases to a maximum and then slowly decreases. In addition, the two independent measurements at the two positions ($x = 5$ mm and 45 mm) on the catalyst confirm that the same results are received based on the two independent measurements, which is necessary for the comparison of local, time-resolved XAS measurements performed sequentially at the respective points.

The bottom line in Fig. 9 now shows the variation of the oxidation state of the catalyst during the measurement and for the two positions on the catalyst. For this purpose, each XANES spectrum was fitted to a linear combination of the reference spectra of the oxidized and reduced catalyst (compare Fig. 8) to obtain the fraction of oxidized Pt species.

The fluctuations in the data points also illustrate clearly the signal-to-noise ratio (SNR) of the time-resolved measurements. The fitting error (3σ interval) at each point is of similar magnitude as the SNR.

Initially, the fraction of oxidized catalyst is about 60%, although it was reduced during pre-treatment. There is evidence of small amounts of residual oxygen still present in the system, most likely from the carrier gas itself, leading to a partial re-oxidation of the catalyst before the actual measurement. Although these residual amounts of oxygen and the partial re-oxidation lead to a higher initial conversion of CO (oxidation to CO_2), they have no further influence on the general phenomena and the decrease in activity over time. As soon as the NO/CO mixture enters the reactor, the catalyst is reduced by CO at the inlet position (x = 5 mm, black circles) for both stoichiometries. The oxidation state falls to values that are very close to the reduced state observed during pre-treatment. At the outlet (x = 45 mm, blue squares), however, the behavior is very different for the two stoichiometries. While the catalyst at the outlet is also immediately reduced by CO under net reducing conditions, the oxidation state under stoichiometric conditions remains at around 60% at the outlet during the entire measurement time and drops only slightly, as indicated by the gray dashed line.

Overall, the XAS measurements indicate that there are strong spatial and even temporal gradients of the catalyst state along the plate under stoichiometric conditions, while the entire catalyst is almost instantaneously reduced in the presence of excess CO. This general behavior is consistent with the spatially resolved catalytic activity derived from PLIF measurements in the gas phase, where we do see complementary spatial and temporal gradients under the same conditions.

4. Discussion

The mechanism of NO reduction by CO involves the adsorption of both NO and CO, the dissociation of adsorbed NO (NO*) and finally the oxidation of adsorbed CO by the adsorbed oxygen from the NO* dissociation [19]. The dissociation of NO* is generally regarded as the rate-determining step. However, dissociation requires the presence of reduced Pt sites, similar to the oxidation of CO by O_2 [19,76,77]. While CO readily reduces Pt sites even at low temperatures, it is also known to inhibit [78] the reaction due to the competitive adsorption of NO and CO in the Langmuir-Hinshelwood type of reaction [14,17,19,79], considering that the adsorption equilibrium constant of CO is almost an order of magnitude larger than that of NO [15]. This is directly reflected in the overall low catalytic activity in the NO/CO reaction over Pt/Al_2O_3 at higher CO concentrations [14,17], leading to the so-called extinguished state, as well as in the negative reaction order with respect to the partial pressure of CO over the catalyst [17,18]. The exact ratio x_{CO}/x_{NO} at which the system enters the extinguished state depends on the absolute concentrations and shifts towards smaller ratios as the CO concentration increases [14,17,28].

The ultimately low conversion as well as the PLIF and XAS results obtained here under net reducing conditions, i.e. with an excess of CO, are at first glance consistent with the known inhibiting effect of CO. The strong adsorption of CO is reflected in the almost immediate reduction of the catalyst over its entire length in less than 2 min with a slight excess of CO (lower right in Fig. 9). Simultaneously, the catalytic activity derived from PLIF decreases uniformly across the catalyst, as shown in Fig. 10, where the ratio $R_{NO}(t,x)/c_{s,NO}(t,x)$ is plotted at selected positions along the catalyst relative to the ratio at $t = 0$ min. Although the rate of decline in activity is the same at each position, it is considerably longer compared to the reduction time scales at the inlet and outlet in the XAS measurements, even though the catalytic plate is twice as long in the XAS studies.

Under stoichiometric conditions, with half the CO content, the behavior is strikingly different as the catalyst is only immediately reduced at the inlet but remains partially oxidized at the outlet (Fig. 9, bottom left). Either the CO concentration at the outlet is now too

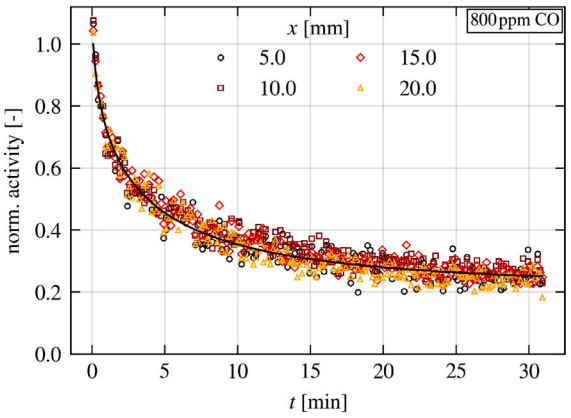

Fig. 10. Visualization of the rate of decline in catalytic activity, represented by the ratio $R_{NO}(t,x)/c_{s,NO}(t,x)$, under net reducing conditions at different positions along the catalytic plate. For a better comparison, the data were normalized to the values at $t = 0$ min for each position separately. (350 °C, 1 L/min, 800 ppm CO, 400 ppm NO, 2% CO_2, rest N_2).

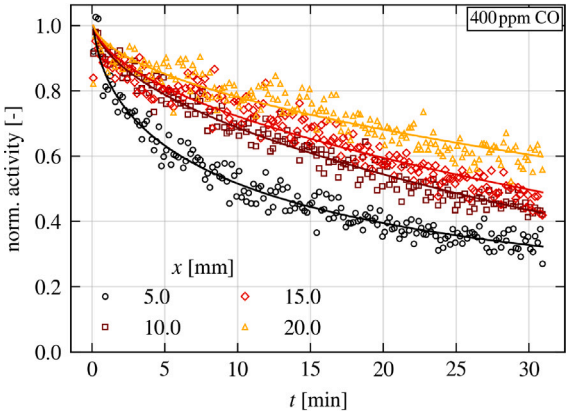

Fig. 11. Visualization of the rate of decline in catalytic activity, represented by the ratio $R_{NO}(t,x)/c_{s,NO}(t,x)$, under stoichiometric conditions at different positions along the catalytic plate. For a better comparison, the data were normalized to the values at $t = 0$ min for each position separately. (350 °C, 1 L/min, 400 ppm CO, 400 ppm NO, 2% CO_2, rest N_2).

low for an efficient reduction and/or the local CO/NO ratio changes significantly along the catalyst to support a more sustained catalytic activity downstream, with a more balanced competitive adsorption of NO and CO at the surface. Indeed, the PLIF measurements show higher activity downstream than upstream, but the activity still decreases over time, albeit much more slowly than with an excess of CO, as shown in Fig. 11. The figure also nicely illustrates the different degradation rates depending on the position on the catalyst.

In analogy to CO oxidation by O_2 [76], NO reduction by CO becomes efficient only when the temperature is high enough and the CO coverage is sufficiently reduced to allow the dissociation of NO to occur efficiently [14,15,17,19]. In other words, the loss of catalytic activity is most likely caused by a gradual loss of active sites over time. While it is known that CO blocks the active sites, the time scales for (a) the reduction of the catalyst upon exposure to CO and (b) the decrease in catalytic activity at different sites of the catalyst are very different. This difference is difficult to explain by CO adsorption alone, especially since CO oxidation and establishing adsorption equilibrium take place on much shorter time scales ($\ll 1$ min) [80]. Another possibility would be that a secondary process counteracts the blocking by CO, such as the generally known formation and storage of isocyanate on the support material [18,25,27,81,82].

A promoting effect of isocyanate formation on the catalytic conversion has first been proposed by Frank and Renken [17], where it maintains some NO and CO consumption and extends the time for the catalyst to reach the steady, extinguished state. After the dissociation of adsorbed NO, CO* can combine with N* to form NCO* (c.f. Scheme 1). Rapid spillover onto the support, where isocyanate is much more stable [25,27,81] effectively removes CO* from the surface thereby releasing reduced Pt sites. Studies on Pt clusters also suggest, that formation of NCO* only occurs in the absence of atomic oxygen [23], which explains why isocyanate is formed only above a certain CO/NO ratio or at low temperatures, where the dissociation of NO* is ineffective.

Many features of –NCO formation on Pt/Al_2O_3 known from the literature are consistent with the temporal–spatial gradients of catalyst state and activity observed here:

1. During the efficient formation of –NCO, two CO molecules are consumed for each NO molecule, leading to a shift of the local CO/NO ratio. Owing to the high formation rate of –NCO and the large storage capacity of alumina, this effect is readily observable even in end-of-pipe measurements [15,18]. Under stoichiometric conditions that shift could be sufficient to push the system locally towards net oxidizing conditions ($x_{CO}/x_{NO} < 1$), thereby reducing the inhibiting effect of CO and resulting in a higher catalytic activity downstream of the catalytic plate.
2. The formation rate of –NCO strongly depends on the stoichiometry and is much faster with an excess of CO (larger CO/NO ratio) [18,27,28,83], similar to the decline in catalytic activity observed here. Additionally, the timescales of both, isocyanate formation and the decline in catalytic activity are very similar [26]. A local shift towards smaller CO/NO ratios under stoichiometric conditions would also explain the slower deactivation rates closer to the outlet.
3. The storage capacity for –NCO on the alumina support is limited [84], so the promoting effect will cease over time as isocyanate accumulates on the support.

Reducing the flow rate by 50% has almost no effect on the rate of decrease in activity over time at the inlet ($x = 5$ mm) and only marginally slows down the deactivation rate at positions further downstream along the plate (see Figure S7 in the supplementary material). The effect of flow rate is therefore negligible compared to the influence of temperature and stoichiometry.

The change in stoichiometry downstream due to –NCO formation would explain the behavior of the chemical state of platinum which can be seen in Fig. 9. Even small amounts of CO under lean conditions below the ignition temperature are known to reduce Pt [85]. Under rich conditions, the abundance of CO immediately leads to a reduction of the catalyst. Even though the CO/NO ratio decreases downstream, the gas phase stays rich which explains why the catalyst bed reduces upstream as well as downstream. Changes in the chemical state of the catalyst in response to a change of the gas phase can occur within seconds [86,87]. The chemical state of the catalyst within the new reactor responds immediately (the measurement after 2 min shows already a reduced state), which shows the capability of the new reactor for tracking fast changes in the catalysts state which is crucial for *operando* investigations that link the activity to the catalysts state.

Under almost stoichiometric (slightly rich) conditions the upstream part of the catalyst is exposed to a rich gas mixture while the downstream part sees a lean mixture. Here CO and NO will compete for adsorption sites on Pt. Support saturation with NCO leads to a decrease in NCO formation and activity, which then leads to an increase in the CO/NO ratio over time. According to the PLIF results this is supposed to happen in a timescale of tens of minutes up to several hours. The slow reduction from an oxidation state of 58% to 52%, observed in Fig. 9 for almost stoichiometric conditions at the downstream position fits this timescale. This confirms that time- and spatially resolved measurements of the gas phase, and the catalysts state measured with the newly designed reactor, can be correlated.

In summary, the influence of isocyanate formation on the local CO/NO ratio as well as its ability to temporarily counteract the inhibiting effect of CO, would explain all the spatial–temporal gradients as well as the timescales at which the catalytic activity and the oxidation state of Pt decline depending on the position along the catalyst.

5. Conclusions

For complex reactions, a spatial and temporal characterization of both the gas phase and the catalyst structure in a reactor is required to promote the development and understanding of current and future catalytic systems. The possibilities of such an approach were demonstrated here using the example of the reduction of NO by CO. Using PLIF, we were able to visualize the spatio-temporal decrease in catalytic activity and derive local conversion rates from the 2D concentration profiles. In addition to the PLIF measurements, the new XAS channel reactor provides time- and spatially-resolved information on the changes in the oxidation state under the same conditions. Whereas CO reduces Pt during the CO/NO reaction under rich conditions with CO-excess and led to a fully reduced Pt at all positions, under stoichiometric conditions a gradient in the Pt oxidation state along the catalyst bed formed with a strong influence on the catalytic activity. For stoichiometric conditions the changes in the oxidation state and the activity profiles for a Pt/Al_2O_3 catalyst during the CO/NO reaction were similar in terms of time and length scales. XAS and PLIF data could well be correlated and supported the possible impact of NCO formation on reaction progress on Pt/Al_2O_3 and the influence of CO poisoning. To replace Rh with Pt, new approaches will be needed to tune the interaction of Pt with CO, e.g. by searching for dopants/bifunctional catalysts or by tailoring lean/rich cycles to convert/release stored NCO. In this context, the combined PLIF/XAS approach presented here is an invaluable tool to investigate and understand the coupling between gas-phase mass transport, catalytic activity and catalyst state under conditions relevant for technical applications.

CRediT authorship contribution statement

Thomas Häber: Writing – review & editing, Writing – original draft, Visualization, Validation, Methodology, Formal analysis, Data curation, Conceptualization. **Sui Wan:** Methodology, Investigation, Data curation. **Samuel Struzek:** Writing – original draft, Investigation, Formal analysis, Data curation. **Camilo Cárdenas:** Writing – review & editing, Investigation, Data curation. **Anna Zimina:** Writing – review & editing, Validation, Investigation, Data curation. **Florian Maurer:** Writing – review & editing, Validation, Supervision, Conceptualization. **Patrick Lott:** Writing – review & editing, Validation, Supervision. **Rainer Suntz:** Writing – review & editing, Supervision. **Jan-Dierk Grunwaldt:** Writing – review & editing, Validation, Supervision, Resources, Project administration, Funding acquisition, Conceptualization. **Olaf Deutschmann:** Writing – review & editing, Validation, Supervision, Resources, Project administration, Funding acquisition, Conceptualization.

Declaration of competing interest

The authors declare that they have no known competing financial interests or personal relationships that could have appeared to influence the work reported in this paper.

Acknowledgments

The financial support of the German Research Foundation (DFG) in the framework of the Collaborative Research Center 1441 (Project-ID 426888090) as well as the Helmholtz program "Materials and Technologies for the Energy Transition, Germany" (MTET, 38.03.04) is gratefully acknowledged. This work was performed with the help of the Large-Scale Data Facility (LSDF) at the Karlsruhe Institute of Technology funded by the Ministry of Science, Research and the Arts Baden-Württemberg and by the Federal Ministry of Education and Research, Germany. Graphics have been prepared with the help of the Matplotlib Python package [88]. The authors thank Joachim Czechowsky (ITCP, KIT) for the preparation of the catalyst, Tim Delrieux (ITCP, KIT) for helping in coating the catalytic plates, Paolo Ciocci (IKFT, KIT) for his support at the CatAct beamline at the KIT Light Source and Sasol Germany GmbH for providing the alumina support material. The authors gratefully acknowledge the Institute for Beam Physics and Technology (IBPT) for operating the storage ring (Karlsruhe Research Accelerator, KARA, and the KIT Light Source), as well as the support provided by instruments at the CAT-ACT beamline from the Institute of Catalysis Research and Technology (IKFT) and the Institute for Chemical Technology and Polymer Chemistry (ITCP).

Appendix A. Supplementary data

Supplementary material related to this article can be found online at https://doi.org/10.1016/j.apcata.2025.120748. The following files are available free of charge as supporting information in the online version.

•supplementary_material.pdf: Additional illustrations and details to support the observations and conclusions made in this work.

Data availability

Data will be made available on request.

References

[1] R.J. Farrauto, M. Deeba, S. Alerasool, Gasoline automobile catalysis and its historical journey to cleaner air, Nat. Catal. 2 (7) (2019) 603–613, http://dx.doi.org/10.1038/s41929-019-0312-9.

[2] M. Votsmeier, T. Kreuzer, J. Gieshoff, G. Lepperhoff, B. Elvers, Automobile exhaust control, in: Ullmann's Encyclopedia of Industrial Chemistry, John Wiley & Sons, Ltd, Weinheim, Germany, 2019, pp. 1–19, http://dx.doi.org/10.1002/14356007.a03_189.pub3.

[3] Z. Liu, F. Yu, C. Ma, J. Dan, J. Luo, B. Dai, A critical review of recent progress and perspective in practical denitration application, Catalysts 9 (9) (2019) 771, http://dx.doi.org/10.3390/catal9090771.

[4] Z. Xu, Y. Li, Y. Lin, T. Zhu, A review of the catalysts used in the reduction of NO by CO for gas purification, Environ. Sci. Pollut. Res. 27 (7) (2020) 6723–6748, http://dx.doi.org/10.1007/s11356-019-07469-w.

[5] Z. Gholami, G. Luo, F. Gholami, F. Yang, Recent advances in selective catalytic reduction of NO_x by carbon monoxide for flue gas cleaning process: A review, Catal. Rev. 63 (1) (2021) 68–119, http://dx.doi.org/10.1080/01614940.2020.1753972.

[6] P. Lott, M. Casapu, J.-D. Grunwaldt, O. Deutschmann, A review on exhaust gas after-treatment of lean-burn natural gas engines – From fundamentals to application, Appl. Catal. B: Environ. 340 (2024) 123241, http://dx.doi.org/10.1016/j.apcatb.2023.123241.

[7] R. Hagan, E. Markey, J. Clancy, M. Keating, A. Donnelly, D.J. O'Connor, L. Morrison, E.J. McGillicuddy, Non-road mobile machinery emissions and regulations: a review, Air 1 (1) (2023) 14–36, http://dx.doi.org/10.3390/air1010002.

[8] M. Sparrevik, X. Qiu, R.A. Stokke, I. Borge, L. de Boer, Investigating the potential for reduced emissions from non-road mobile machinery in construction activities through disruptive innovation, Environ. Technol. Innov. 31 (2023) 103187, http://dx.doi.org/10.1016/j.eti.2023.103187.

[9] P. Granger, F. Dhainaut, S. Pietrzik, P. Malfoy, A.S. Mamede, L. Leclercq, G. Leclercq, An overview: Comparative kinetic behaviour of Pt, Rh and Pd in the NO+CO and NO+H_2 reactions, Top. Catal. 39 (1) (2006) 65–76, http://dx.doi.org/10.1007/s11244-006-0039-0.

[10] A. Srinivasan, C. Depcik, Review of chemical reactions in the NO reduction by CO on Rhodium/Alumina catalysts, Catal. Rev. 52 (4) (2010) 462–493, http://dx.doi.org/10.1080/01614940.2010.522485.

[11] A. Cowley, "PGM Market Report May 2023": A return to more balanced conditions is expected, Johns. Matthey Technol. Rev. 67 (3) (2023) 361–363, http://dx.doi.org/10.1595/205651323X16856083453770.

[12] G. Fisher, M. Zammit, W. Labarge, Investigation of catalytic alternatives to rhodium in emissions control, SAE Tech. Pap. 920846 (1992) http://dx.doi.org/10.4271/920846.

[13] L. Castoldi, L. Lietti, R. Bonzi, N. Artioli, P. Forzatti, S. Morandi, G. Ghiotti, The NOx Reduction by CO on a Pt-K/Al_2O_3 Lean NO_x Trap Catalyst, J. Phys. Chem. C 115 (4) (2011) 1277–1286, http://dx.doi.org/10.1021/jp106753g.

[14] A. Srinivasan, C. Depcik, Review of chemical reactions in the NO reduction by CO on platinum/alumina catalysts, Surf. Rev. Lett. 19 (01) (2012) 1230001, http://dx.doi.org/10.1142/S0218625X12300018.

[15] P. Granger, C. Dathy, J.J. Lecomte, L. Leclercq, M. Prigent, G. Mabilon, G. Leclercq, Kinetics of the NO and CO reaction over platinum catalysts: I. Influence of the support, J. Catalysis 173 (2) (1998) 304–314, http://dx.doi.org/10.1006/jcat.1997.1932.

[16] H. Muraki, Y. Fujitani, Nitric oxide reduction by carbon monoxide over noble-metal catalysts under cycled feedstreams, Ind. Eng. Chem. Prod. Res. Dev. 25 (3) (1986) 414–419, http://dx.doi.org/10.1021/i300023a008.

[17] B. Frank, A. Renken, Kinetics and deactivation of the NO reduction by CO on Pt-supported catalysts, Chem. Eng. Technol. 22 (6) (1999) 490–494, http://dx.doi.org/10.1002/(SICI)1521-4125(199906)22:6<490::AID-CEAT490>3.0.CO;2-9.

[18] D. Lorimer, A.T. Bell, Reduction of NO by CO over a silica-supported platinum catalyst: Infrared and kinetic studies, J. Catalysis 59 (2) (1979) 223–238, http://dx.doi.org/10.1016/S0021-9517(79)80027-5.

[19] R.R. Sadhankar, D.T. Lynch, NO reduction by CO over a Pt/Al_2O_3 catalyst: Reaction kinetics and experimental bifurcation behavior, Ind. Eng. Chem. Res. 36 (11) (1997) 4609–4619, http://dx.doi.org/10.1021/ie970138z.

[20] D. Mantri, P. Aghalayam, Detailed surface reaction mechanism for reduction of NO by CO, Catal. Today 119 (1) (2007) 88–93, http://dx.doi.org/10.1016/j.cattod.2006.08.002.

[21] J.-L. Freysz, J. Saussey, J.-C. Lavalley, P. Bourges, In situ FTIR study of the NO+CO reaction on a silica-supported platinum catalyst at atmospheric pressure using a new pulse technique, J. Catalysis 197 (1) (2001) 131–138, http://dx.doi.org/10.1006/jcat.2000.3060.

[22] Y.J. Mergler, B.E. Nieuwenhuys, NO reduction by CO over Pt/Al_2O_3 and Pt/CeO_x/Al_2O_3: oscillations and deactivation, J. Catalysis 161 (1) (1996) 292–303, http://dx.doi.org/10.1006/jcat.1996.0187.

[23] E. Fernández, L. Liu, M. Boronat, R. Arenal, P. Concepcion, A. Corma, Low-temperature catalytic NO reduction with CO by subnanometric Pt clusters, ACS Catal. 9 (12) (2019) 11530–11541, http://dx.doi.org/10.1021/acscatal.9b03207.

[24] Q. Zhang, L. Lv, J. Zhu, X. Wang, J. Wang, M. Shen, The effect of CO on NO reduction over Pt/Pd-based NSR catalysts at low temperature, Catal. Sci. Technol. 3 (4) (2013) 1069–1077, http://dx.doi.org/10.1039/C2CY20775C.

[25] M.L. Unland, Isocyanate intermediates in the reaction nitrogen monoxide + carbon monoxide over a platinum/aluminum oxide catalyst, J. Phys. Chem. 77 (16) (1973) 1952–1956, http://dx.doi.org/10.1021/j100635a006.

[26] H. Niiyama, M. Tanaka, H. Iida, E. Echigoya, Infrared studies of the isocyanate species formed in the reaction of NO with CO over Pt and Rh, Bull. Chem. Soc. Japan 49 (8) (1976) 2047–2050, http://dx.doi.org/10.1246/bcsj.49.2047.

[27] F. Solymosi, L. Völgyesi, J. Sárkány, The effect of the support on the formation and stability of surface isocyanate on platinum, J. Catalysis 54 (3) (1978) 336–344, http://dx.doi.org/10.1016/0021-9517(78)90081-7.

[28] C.C. Chang, L.L. Hegedus, Surface reactions of NO, CO, and O_2 near the stoichiometric point: I. Pt-alumina, J. Catalysis 57 (3) (1979) 361–371, http://dx.doi.org/10.1016/0021-9517(79)90002-2.

[29] L.L. Hegedus, C.C. Chang, D.J. McEwen, E.M. Sloan, Response of catalyst surface concentrations to forced concentration oscillations in the gas phase. The NO, CO, O_2 system over Pt-Alumina, Ind. Eng. Chem. Fundam. 19 (4) (1980) 367–373, http://dx.doi.org/10.1021/i160076a008.

[30] P. Xiao, R.C. Davis, X. Ouyang, J. Li, A. Thomas, S.L. Scott, J. Zhu, Mechanism of NO reduction by CO over Pt/SBA-15, Catal. Commun. 50 (2014) 69–72, http://dx.doi.org/10.1016/j.catcom.2014.02.027.

[31] G. Kychakoff, R.D. Howe, R.K. Hanson, J.C. McDaniel, Quantitative visualization of combustion species in a plane, Appl. Opt. 21 (18) (1982) 3225–3227, http://dx.doi.org/10.1364/AO.21.003225.

[32] R.K. Hanson, J.M. Seitzman, P.H. Paul, Planar laser-fluorescence imaging of combustion gases, Appl. Phys. B 50 (6) (1990) 441–454, http://dx.doi.org/10.1007/BF00408770.

[33] C. Schulz, V. Sick, Tracer-LIF diagnostics: Quantitative measurement of fuel concentration, temperature and fuel/air ratio in practical combustion systems, Prog. Energy Combust. Sci. 31 (1) (2005) 75–121, http://dx.doi.org/10.1016/j.pecs.2004.08.002.

[34] J.H. Frank, Advances in imaging of chemically reacting flows, J. Chem. Phys. 154 (4) (2021) 040901, http://dx.doi.org/10.1063/5.0028249.

[35] M. Reinke, J. Mantzaras, R. Bombach, S. Schenker, A. Inauen, Gas phase chemistry in catalytic combustion of methane/air mixtures over platinum at pressures of 1 to 16 bar, Combust. Flame 141 (4) (2005) 448–468, http://dx.doi.org/10.1016/j.combustflame.2005.01.016.

[36] J. Mantzaras, R. Bombach, R. Schaeren, Hetero-/homogeneous combustion of hydrogen/air mixtures over platinum at pressures up to 10bar, Proc. Combust. Inst. 32 (2) (2009) 1937–1945, http://dx.doi.org/10.1016/j.proci.2008.06.067.

[37] A. Zellner, R. Suntz, O. Deutschmann, Two-dimensional spatial resolution of concentration profiles in catalytic reactors by planar laser-induced fluorescence: NO reduction over diesel oxidation catalysts, Angew. Chem. Int. Ed. 54 (9) (2015) 2653–2655, http://dx.doi.org/10.1002/anie.201410324.

[38] J. Zetterberg, S. Blomberg, J. Gustafson, J. Evertsson, J. Zhou, E.C. Adams, P.-A. Carlsson, M. Aldén, E. Lundgren, Spatially and temporally resolved gas distributions around heterogeneous catalysts using infrared planar laser-induced fluorescence, Nat. Commun. 6 (1) (2015) 7076, http://dx.doi.org/10.1038/ncomms8076.

[39] S. Blomberg, J. Zhou, J. Gustafson, J. Zetterberg, E. Lundgren, 2D and 3D imaging of the gas phase close to an operating model catalyst by planar laser induced fluorescence, J. Phys.: Condens. Matter. 28 (45) (2016) 453002, http://dx.doi.org/10.1088/0953-8984/28/45/453002.

[40] J. Zhou, S. Pfaff, E. Lundgren, J. Zetterberg, A convenient setup for laser-induced fluorescence imaging of both CO and CO_2 during catalytic CO oxidation, Appl. Phys. B 123 (3) (2017) 87, http://dx.doi.org/10.1007/s00340-017-6681-3.

[41] J. Zhou, S. Blomberg, J. Gustafson, E. Lundgren, J. Zetterberg, Visualization of gas distribution in a model AP-XPS reactor by PLIF: CO oxidation over a Pd(100) catalyst, Catalysts 7 (1) (2017) 29, http://dx.doi.org/10.3390/catal7010029.

[42] S. Blomberg, J. Zetterberg, J. Gustafson, J. Zhou, M. Shipilin, S. Pfaff, U. Hejral, P.-A. Carlsson, O. Gutowski, F. Bertram, E. Lundgren, Combining synchrotron light with laser technology in catalysis research, J. Synchrotron Radiat. 25 (5) (2018) 1389–1394, http://dx.doi.org/10.1107/S1600577518010597.

[43] J. Mantzaras, Progress in non-intrusive laser-based measurements of gas-phase thermoscalars and supporting modeling near catalytic interfaces, Prog. Energy Combust. Sci. 70 (2019) 169–211, http://dx.doi.org/10.1016/j.pecs.2018.10.005.

[44] S. Wan, Y. Guo, T. Häber, R. Suntz, O. Deutschmann, Spatially and temporally resolved measurements of NO adsorption/desorption over NOx-storage catalyst, ChemPhysChem 21 (23) (2020) 2497–2501, http://dx.doi.org/10.1002/cphc.202000765.

[45] S. Wan, B. Torkashvand, T. Häber, R. Suntz, O. Deutschmann, Investigation of HCHO catalytic oxidation over platinum using planar laser-induced fluorescence, Appl. Catal. B: Environ. 264 (2020) 118473, http://dx.doi.org/10.1016/j.apcatb.2019.118473.

[46] J. Mantzaras, R. Sui, C.K. Law, R. Bombach, Heterogeneous and homogeneous combustion of fuel-lean $C_3H_8/O_2/N_2$ mixtures over rhodium at pressures up to 6 bar, Proc. Combust. Inst. 38 (4) (2021) 6473–6482, http://dx.doi.org/10.1016/j.proci.2020.06.029.

[47] B. Zhou, E. Huang, R. Almeida, S. Gurses, A. Ungar, J. Zetterberg, A. Kulkarni, C.X. Kronawitter, D.L. Osborn, N. Hansen, J.H. Frank, Near-surface imaging of the multicomponent gas phase above a silver catalyst during partial oxidation of methanol, ACS Catal. 11 (1) (2021) 155–168, http://dx.doi.org/10.1021/acscatal.0c04396.

[48] D. van den Bekerom, C. Richards, E. Huang, I. Adamovich, J.H. Frank, 2D imaging of absolute methyl concentrations in nanosecond pulsed plasma by photo-fragmentation laser-induced fluorescence, Plasma Sources Sci. Technol. 31 (9) (2022) 095018, http://dx.doi.org/10.1088/1361-6595/ac8f6c.

[49] S. Wan, K. Keller, P. Lott, A.B. Shirsath, S. Tischer, T. Häber, R. Suntz, O. Deutschmann, Experimental and numerical investigation of NO oxidation on Pt/Al_2O_3- and NO_x storage on $Pt/BaO/Al_2O_3$-catalysts, Catal. Sci. Technol. 12 (14) (2022) 4456–4470, http://dx.doi.org/10.1039/D2CY00572G.

[50] S. Wan, T. Häber, P. Lott, R. Suntz, O. Deutschmann, Experimental investigation of NO reduction by H_2 on Pd using planar laser-induced fluorescence, Appl. Energy Combust. Sci. (2023) 100229, http://dx.doi.org/10.1016/j.jaecs.2023.100229.

[51] W.P. Partridge, J.M.E. Storey, S.A. Lewis, R.W. Smithwick, G.L. DeVault, M.J. Cunningham, N.W. Currier, T.M. Yonushonis, Time-resolved measurements of emission transients by mass spectrometry, SAE Technical Paper 2000-01-2952, SAE International, Warrendale, PA, 2000, http://dx.doi.org/10.4271/2000-01-2952.

[52] R. Horn, O. Korup, M. Geske, U. Zavyalova, I. Oprea, R. Schlögl, Reactor for in situ measurements of spatially resolved kinetic data in heterogeneous catalysis, Rev. Sci. Instrum. 81 (6) (2010) 064102, http://dx.doi.org/10.1063/1.3428727.

[53] A. Donazzi, D. Livio, M. Maestri, A. Beretta, G. Groppi, E. Tronconi, P. Forzatti, Synergy of homogeneous and heterogeneous chemistry probed by in situ spatially resolved measurements of temperature and composition, Angew. Chem. Int. Ed. 50 (17) (2011) 3943–3946, http://dx.doi.org/10.1002/anie.201007346.

[54] D. Livio, C. Diehm, A. Donazzi, A. Beretta, O. Deutschmann, Catalytic partial oxidation of ethanol over Rh/Al_2O_3: Spatially resolved temperature and concentration profiles, Appl. Catal. A: Gen. 467 (2013) 530–541, http://dx.doi.org/10.1016/j.apcata.2013.07.054.

[55] C. Diehm, H. Karadeniz, C. Karakaya, M. Hettel, O. Deutschmann, Chapter two - spatial resolution of species and temperature profiles in catalytic reactors: In situ sampling techniques and CFD Modeling, in: A.G. Dixon (Ed.), Advances in Chemical Engineering, in: Modeling and Simulation of Heterogeneous Catalytic Processes, vol. 45, Academic Press, 2014, pp. 41–95, http://dx.doi.org/10.1016/B978-0-12-800422-7.00002-9.

[56] J.N. Bär, C. Karakaya, O. Deutschmann, Catalytic ignition of light hydrocarbons over Rh/Al_2O_3 studied in a stagnation-point flow reactor, Proc. Combust. Inst. 34 (2) (2013) 2313–2320, http://dx.doi.org/10.1016/j.proci.2012.06.115.

[57] S.M. Gurses, N. Felvey, L.R. Filardi, A.J. Zhang, J. Wood, K. van Benthem, J.H. Frank, D.L. Osborn, N. Hansen, C.X. Kronawitter, Constraining reaction pathways for methanol oxidation through operando interrogation of both the surface and the near-surface gas phase, Chem Catal. 3 (10) (2023) 100782, http://dx.doi.org/10.1016/j.checat.2023.100782.

[58] S. Struzek, T. Delrieux, F. Maurer, D.S. Gonçalves, S.-L. Heck, L. Klag, J. Czechowsky, A. Zimina, J.-D. Grunwaldt, Role of powders and coatings for relating catalytic activity and structure of Pt in emission control catalysis, React. Chem. Eng. 10 (6) (2025) 1233–1243, http://dx.doi.org/10.1039/D4RE00262H.

[59] A.M. Gänzler, M. Casapu, D.E. Doronkin, F. Maurer, P. Lott, P. Glatzel, M. Votsmeier, O. Deutschmann, J.-D. Grunwaldt, Unravelling the different reaction pathways for low temperature CO oxidation on Pt/CeO_2 and Pt/Al_2O_3 by spatially resolved structure–activity correlations, J. Phys. Chem. Lett. 10 (24) (2019) 7698–7705, http://dx.doi.org/10.1021/acs.jpclett.9b02768.

[60] L. Klag, T.L. Sheppard, J.-D. Grunwaldt, An advanced characterization toolbox for selective olefin oxidation catalysts, ChemCatChem 15 (3) (2023) e202201276, http://dx.doi.org/10.1002/cctc.202201276.

[61] B.B. Sarma, F. Maurer, D.E. Doronkin, J.-D. Grunwaldt, Design of single-atom catalysts and tracking their fate using *Operando* and advanced X-ray spectroscopic tools, Chem. Rev. 123 (1) (2023) 379–444, http://dx.doi.org/10.1021/acs.chemrev.2c00495.

[62] B.B. Sarma, J.-D. Grunwaldt, Operando spectroscopy to understand dynamic structural changes of solid catalysts, CHIMIA 78 (5) (2024) 288–296, http://dx.doi.org/10.2533/chimia.2024.288.

[63] J.-D. Grunwaldt, J.B. Wagner, R.E. Dunin-Borkowski, Imaging catalysts at work: A hierarchical approach from the macro- to the meso- and nano-scale, ChemCatChem 5 (1) (2013) 62–80, http://dx.doi.org/10.1002/cctc.201200356.

[64] J. Becher, D.F. Sanchez, D.E. Doronkin, D. Zengel, D.M. Meira, S. Pascarelli, J.-D. Grunwaldt, T.L. Sheppard, Chemical gradients in automotive Cu-SSZ-13 catalysts for NOx removal revealed by operando X-ray spectrotomography, Nat. Catal. 4 (1) (2021) 46–53, http://dx.doi.org/10.1038/s41929-020-00552-3.

[65] W. Kleist, J.-D. Grunwaldt, High output catalyst development in heterogeneous gas phase catalysis, in: A. Hagemeyer, A. Volpe (Eds.), Modern Applications of High Throughput R&D in Heterogeneous Catalysis, Bentham Science Publishers, 2014, pp. 357–371, http://dx.doi.org/10.2174/9781608058723114010018.

[66] F. Maurer, J. Jelic, J. Wang, A. Gänzler, P. Dolcet, C. Wöll, Y. Wang, F. Studt, M. Casapu, J.-D. Grunwaldt, Tracking the formation, fate and consequence for catalytic activity of Pt single sites on CeO_2, Nat. Catal. 3 (10) (2020) 824–833, http://dx.doi.org/10.1038/s41929-020-00508-7.

[67] G. Bergeret, P. Gallezot, Particle size and dispersion measurements, in: Handbook of Heterogeneous Catalysis, John Wiley & Sons, Ltd, Weinheim, Germany, 2008, pp. 738–765, http://dx.doi.org/10.1002/9783527610044.hetcat0038.

[68] W.G. Bessler, C. Schulz, T. Lee, J.B. Jeffries, R.K. Hanson, Strategies for laser-induced fluorescence detection of nitric oxide in high-pressure flames. III. Comparison of A–X excitation schemes, Appl. Opt. 42 (24) (2003) 4922–4936, http://dx.doi.org/10.1364/AO.42.004922.

[69] P.H. Paul, J.A. Gray, J.L. Durant, J.W. Thoman, Collisional quenching corrections for laser-induced fluorescence measurements of NO $A^2\Sigma^+$, AIAA J. 32 (8) (1994) 1670–1675, http://dx.doi.org/10.2514/3.12158.

[70] A. Zimina, K. Dardenne, M.A. Denecke, D.E. Doronkin, E. Huttel, H. Lichtenberg, S. Mangold, T. Pruessmann, J. Rothe, T. Spangenberg, R. Steininger, T. Vitova, H. Geckeis, J.-D. Grunwaldt, CAT-ACT—A new highly versatile x-ray spectroscopy beamline for catalysis and radionuclide science at the KIT synchrotron light facility ANKA, Rev. Sci. Instrum. 88 (11) (2017) 113113, http://dx.doi.org/10.1063/1.4999928.

[71] K.Y.S. Ng, D.N. Belton, S.J. Schmieg, G.B. Fisher, NO-CO activity and selectivity over a $Pt_{10}Rh_{90}$(111) alloy catalyst in the 10-torr pressure range, J. Catalysis 146 (2) (1994) 394–406, http://dx.doi.org/10.1006/jcat.1994.1077.

[72] L. Kubiak, L. Righini, L. Castoldi, R. Matarrese, P. Forzatti, L. Lietti, M. Daturi, Mechanistic aspects of N_2O formation over Pt-based lean NO_x trap catalysts, Top. Catal. 59 (10) (2016) 976–981, http://dx.doi.org/10.1007/s11244-016-0577-z.

[73] L. Kantorovich, Partial differential equations of mathematical physics, in: L. Kantorovich (Ed.), Mathematics for Natural Scientists II: Advanced Methods, in: Undergraduate Lecture Notes in Physics, Springer International Publishing, Cham, 2016, pp. 545–608, http://dx.doi.org/10.1007/978-3-319-27861-2_8.

[74] D.G. Goodwin, H.K. Moffat, I. Schoegl, R.L. Speth, B.W. Weber, Cantera: An object-oriented software toolkit for chemical kinetics, thermodynamics, and transport processes, 2023, http://dx.doi.org/10.5281/ZENODO.8137090, Zenodo.

[75] J. Bzowski, J. Kestin, E.A. Mason, F.J. Uribe, Equilibrium and transport properties of gas mixtures at low density: eleven polyatomic gases and five noble gases, J. Phys. Chem. Ref. Data 19 (5) (1990) 1179–1232, http://dx.doi.org/10.1063/1.555867.

[76] M.A. Newton, D. Ferri, G. Smolentsev, V. Marchionni, M. Nachtegaal, Room-temperature carbon monoxide oxidation by oxygen over Pt/Al_2O_3 mediated by reactive platinum carbonates, Nat. Commun. 6 (1) (2015) 8675, http://dx.doi.org/10.1038/ncomms9675.

[77] A. Boubnov, A. Gänzler, S. Conrad, M. Casapu, J.-D. Grunwaldt, Oscillatory CO oxidation over Pt/Al_2O_3 catalysts studied by In situ XAS and DRIFTS, Top. Catal. 56 (1) (2013) 333–338, http://dx.doi.org/10.1007/s11244-013-9976-6.

[78] P. Forzatti, L. Lietti, Catalyst deactivation, Catal. Today 52 (2) (1999) 165–181, http://dx.doi.org/10.1016/S0920-5861(99)00074-7.

[79] M. Di, A. Schaefer, F. Hemmingsson, T. Bell, Y. Feng, M. Skoglundh, D. Thompsett, P.-A. Carlsson, Why nitrogen oxide inhibits CO oxidation over highly dispersed platinum ceria catalysts, Catal. Today 426 (2024) 114394, http://dx.doi.org/10.1016/j.cattod.2023.114394.

[80] T. Engel, G. Ertl, Elementary steps in the catalytic oxidation of carbon monoxide on platinum metals, in: D.D. Eley, H. Pines, P.B. Weez (Eds.), Advances in Catalysis, vol. 28, Academic Press Inc., Cambridge, Massachusetts, USA, 1979, pp. 1–78, http://dx.doi.org/10.1016/S0360-0564(08)60133-9.

[81] F. Solymosi, J. Sárkány, A. Schauer, Study of the formation of isocyanate surface complexes on Pt/Al_2O_3 catalysts, J. Catalysis 46 (3) (1977) 297–307, http://dx.doi.org/10.1016/0021-9517(77)90213-5.

[82] J. Raskó, F. Solymosi, Infrared study of the formation and stability of isocyanate species on some unsupported noble metals, J. Catalysis 71 (1) (1981) 219–222, http://dx.doi.org/10.1016/0021-9517(81)90220-7.

[83] F. Solymosi, J. Kiss, J. Sarkany, On the reactions of surface isocyanate over platinum catalyst, in: Proceedings 3rd International Conference on Solid Surfaces, Vol. 1, 1977, pp. 819–822.

[84] M. Barreau, X. Courtois, F. Can, FT-IR spectroscopy study of HNCO adsorption and hydrolysis over oxide-based samples dedicated to $deNO_x$ processes, Appl. Catal. A: Gen. 552 (2018) 147–153, http://dx.doi.org/10.1016/j.apcata.2017.12.019.

[85] M. Casapu, A. Fischer, A.M. Gänzler, R. Popescu, M. Crone, D. Gerthsen, M. Türk, J.-D. Grunwaldt, Origin of the normal and inverse hysteresis behavior during CO oxidation over Pt/Al_2O_3, ACS Catal. 7 (1) (2017) 343–355, http://dx.doi.org/10.1021/acscatal.6b02709.

[86] F. Maurer, A. Gänzler, P. Lott, B. Betz, M. Votsmeier, S. Loridant, P. Vernoux, V. Murzin, B. Bornmann, R. Frahm, O. Deutschmann, M. Casapu, J.-D. Grunwaldt, Spatiotemporal investigation of the temperature and structure of a Pt/CeO_2 oxidation catalyst for CO and hydrocarbon oxidation during pulse activation, Ind. Eng. Chem. Res. 60 (18) (2021) 6662–6675, http://dx.doi.org/10.1021/acs.iecr.0c05798.

[87] A.M. Gänzler, M. Casapu, F. Maurer, H. Störmer, D. Gerthsen, G. Ferré, P. Vernoux, B. Bornmann, R. Frahm, V. Murzin, M. Nachtegaal, M. Votsmeier, J.-D. Grunwaldt, Tuning the Pt/CeO_2 interface by in situ variation of the Pt particle size, ACS Catal. 8 (6) (2018) 4800–4811, http://dx.doi.org/10.1021/acscatal.8b00330.

[88] J.D. Hunter, Matplotlib: A 2D graphics environment, Comput. Sci. Eng. 9 (3) (2007) 90–95, http://dx.doi.org/10.1109/MCSE.2007.55.